Gosalawit-Utke, R.; Milanese, C.; Javadian, P.; Jepsen, J.; Laipple, D.;
Karmi, F.; Puszkiel, J.; Jensen, T.R.; Marini, A.; Klassen, T.; Dornheim, M.:

Nanoconfined 2LiBH4–MgH2–TiCl3 in carbon aerogel scaffold for reversible hydrogen storage

In: International Journal of Hydrogen Energy (2013) Elsevier

DOI: 10.1016/j.ijhydene.2012.12.123

Nanoconfined $2LiBH_4–MgH_2–TiCl_3$ in Carbon Aerogel Scaffold for Reversible Hydrogen Storage

Rapee Gosalawit–Utke[1, 2, *], Chiara Milanese[3], Payam Javadian[4], Julian Jepsen[1], Daniel Laipple[1], Fahim Karmi[1], Julian Puszkeil[1], Torben R. Jensen[4], Amedeo Marini[3], Thomas Klassen[1], Martin Dornheim[1]

[1]Institute of Materials Research, Materials Technology, Helmholtz–Zentrum Geesthacht, Geesthacht21502, Germany.

[2]School of Chemistry, Institute of Science, Suranaree University of Technology, Nakhon Ratchasima 30000, Thailand, Email: rapee.g@sut.ac.th.

[3]Pavia Hydrogen Lab, C. S.G. I.–Department of Chemistry–Physical Chemistry Division, University of Pavia, Pavia 27100, Italy.

[4]Center for Energy Materials, iNANO and Department of Chemistry, University of Aarhus, Aarhus C8000, Denmark.

Nanoconfinement of $2LiBH_4–MgH_2–TiCl_3$ in resorcinol–formaldehyde carbon aerogel scaffold (RF–CAS) for reversible hydrogen storage applications is proposed. RF–CAS is encapsulated with approximately 1.6 wt. % $TiCl_3$ by solution impregnation technique, and it is further nanoconfined with bulk $2LiBH_4–MgH_2$ via melt infiltration. Faster dehydrogenation kinetics is obtained after $TiCl_3$ impregnation, for example, nanoconfined $2LiBH_4–MgH_2–TiCl_3$ requires ~ 1 and 4.5 h, respectively, to release 95 % of the total hydrogen content during the 1st and 2nd cycles, while nanoconfined $2LiBH_4–MgH_2$ (~ 2.5 and 7 h, respectively) and bulk material (~ 23 and 22 h, respectively) take considerably longer. Moreover, 95–98.6 % of the theoretical H_2 storage capacity (3.6–3.75 wt. % H_2) is reproduced after four hydrogen release and uptake cycles of the nanoconfined $2LiBH_4–MgH_2–TiCl_3$. The reversibility of this hydrogen storage material is confirmed by the formation of $LiBH_4$ and MgH_2 after rehydrogenation using FTIR and SR–PXD techniques, respectively.

*Corresponding author

Keywords: nanoconfinement, carbon aerogel scaffold, hydrogen storage, lithium borohydride, magnesium hydride, titanium trichloride.

1. Introduction

Nanostructuring based on size reduction of the solid–state metal or complex hydrides for reversible hydrogen storages is currently of interest. Several research groups have revealed that the nanoscale significantly affects the hydrogen exchange kinetics and thermodynamic destabilization of hydride materials [1–5]. The high–energy ball milling technique is conventionally used to decrease the crystallite size and allow catalytic doping of inorganic materials [3, 6]. Nanoparticles of various hydride materials (with and without additives), such as metal hydrides (e.g., MgH_2–TiH_2 [7–8]), complex hydrides (e.g., $LiBH_4$–oxide additives [9] and $LiBH_4$–Mg [10]), and reactive hydride composites (e.g., $2LiBH_4$–MgH_2 [3, 11] and $2LiBH_4$–MgH_2–transition metal chlorides [12]), have been ball milled for reversible hydrogen storage applications. Nevertheless, repeated hydrogen release and uptake cycles at elevated temperatures result in grain growth and particle agglomeration [13]. In this regard, to keep the hydride particles at nanosizes during de–/rehydrogenation cycles, nanoporous carbon aerogel scaffolds have been recently used for hydride confinements due to their chemical inertness, light weight, and controllable pore size.

Confinement of metal hydride, e.g., MgH_2, in nanoporous carbon hosts, was carried out by various means, such as the melt infiltration of metallic Mg into Ni– or Cu–deposited carbon scaffold and hydrogenation of Mg to MgH_2 [14]. In addition, encapsulation of magnesium dibutyl ($MgBu_2$) precursor in carbon aerogel by solution impregnation and hydrogenation ($p(H_2)$= 50 bar and T=170 °C) to MgH_2 was also reported elsewhere [15–16]. Nanoconfined MgH_2 revealed a significant improvement in hydrogen sorption kinetics as compared with bulk MgH_2. For instance, MgH_2 infiltrated in Ni–deposited carbon aerogel released hydrogen at an average rate of 25 wt. % h^{-1}, while that of ball–milled MgH_2 with graphite was 0.12 wt. % h^{-1}

[14]. Not only metal hydrides, but also complex hydrides have been infiltrated in nanoporous carbon aerogels, and they presented superior kinetics as compared with ball–milled materials. Nanoconfined $NaAlH_4$ prepared by melt infiltration showed a single–step dehydrogenation at low temperatures as well as rehydrogenation at mild condition (e.g., 24 bar H_2 at 150 °C) [17]. Besides, a lot of attention has been focused on the confinement of $LiBH_4$ in nanoporous carbon aerogel scaffold, due to its high gravimetric H_2 storage capacity (18.5 wt. %) [5]. Simultaneously, nanoconfinements of reactive hydride composites (e.g., $2LiBH_4$–MgH_2 [4, 18–19], $2NaBH_4$–MgH_2 [20], and $LiBH_4$–$Ca(BH_4)_2$ [21]) have also been carried out. All of them showed a considerable improvement in hydrogen sorption kinetics. For example, nanoconfined $2LiBH_4$–MgH_2 in resorcinol–formaldehyde carbon aerogel released hydrogen ten times faster than the bulk sample during the 1st dehydrogenation [4]. Moreover, instead of a normal two–step dehydrogenation, a single–step reaction was obtained from $2LiBH_4$–MgH_2 after nanoconfinement, suggesting that the thermodynamics had changed [4, 18]. Furthermore, catalytic doping in the nanoconfined hydride sample was performed to improve its kinetic properties. Nielsen et al. [22] reported that nanoconfinement of $NaAlH_4$ in carbon aerogel catalyzed with 3.0 wt. % $TiCl_3$ showed superior dehydrogenation kinetics over both nanoconfined $NaAlH_4$ (without catalyst) and bulk $NaAlH_4$–$TiCl_3$.

On the basis of $2LiBH_4$–MgH_2 composite, it is well known that various additives, such as $TiCl_3$, $ZrCl_4$, VCl_3 [12, 23], TiO_2 [24], and Nb_2O_5 [25] have been loaded to optimize the reaction performance during de–/rehydrogenation. In the present study, we extend our previous research by focusing on kinetic improvement of the nanoconfined $2LiBH_4$–MgH_2 in carbon aerogel scaffold by catalytic doping. Prior to melt infiltration of $2LiBH_4$–MgH_2, titanium trichloride ($TiCl_3$) is impregnated in carbon aerogel scaffold prepared from resorcinol–formaldehyde (RF) aerogel. Nanoconfinements of both hydride composite and catalyst are confirmed by N_2 adsorption–desorption measurements, scanning electron microscopy (SEM), and energy dispersive X–ray spectroscopy (EDS). Dehydrogenation, reversibility, reaction mechanisms, and kinetics of both nanoconfined samples (with and without $TiCl_3$) are determined by *in situ* synchrotron radiation powder X–ray diffraction (SR–PXD), Fourier transform infrared spectroscopy (FTIR), coupled manometric–calorimetric measurements, and titration experiments.

2. Experimental details

2.1. Sample preparation

The powder samples of 4.52 g $LiBH_4$ (90+ % hydrogen–storage grade, Aldrich) and 2.67 g MgH_2 (hydrogen–storage grade, Aldrich) were milled in a 2:1 mole ratio using a Fritsch Pulverisette 6 classic line planetary mill under an argon atmosphere in a glove box. The mixture was milled in a stainless steel vial (Evico Magnetic, Germany) with a ball–to–powder weight ratio (BPR) of 10:1. Milling was performed for 5 h at 400 rpm to obtain bulk $2LiBH_4$–MgH_2.

Resorcinol–formaldehyde (RF) aerogels were prepared according to the previous procedures [5, 26]. The aerogel was synthesized by mixing 41.4286 g of resorcinol (99 %, Aldrich), 56.64 ml deionized water, 56.92 ml of a 37 wt. % formaldehyde in a water solution stabilized by 10–15 wt. % methanol, and 0.0337 g of Na_2CO_3 (Aldrich, 99.999%) in a beaker under continuous stirring until homogeneity. The polymer solution was poured into polypropylene bottles and sealed with the lids. The solution was aged at room temperature for 24 h, at 50 $^{\circ}$C for 24 h, at 90°C for 72 h, and cooled to room temperature in ambient condition. The aerogel obtained was soaked in an acetone bath three times within a period of 3–4 days and dried at room temperature for several days inside the fume hood. The monolith of gels was cut into smaller pieces of ca. 0.4 cm^3 for further carbonization. The pieces of monolithic aerogel were carbonized in a tubular oven at a constant temperature of 800 $^{\circ}$C (heating rate of 2.6 $^{\circ}$C/min) for 6 h under nitrogen flow. The furnace was turned off, and the samples were left to cool to room temperature. The gel obtained was dried at 500 °C under vacuum for 16 h to achieve an RF carbon aerogel scaffold, denoted as RF–CAS.

The impregnation of titanium trichloride ($TiCl_3$) (>99.99 % hydrogen–storage grade, Aldrich) in RF–CAS was carried out by (i) dissolving 0.0406 g $TiCl_3$ in 30 mL dried acetone (≥99.9 %, Aldrich) to obtain 5.4 wt. % $TiCl_3$ solution; (ii) immersing 1.1636 g RF–CAS in $TiCl_3$ solution; and (iii) drying RF–CAS at room temperature in a glove box for several days. As the acetone evaporated, 1.1822 g of $TiCl_3$–impregnated RF–CAS (1.6 wt. % $TiCl_3$ in RF–CAS) was obtained and denoted as $TiCl_3$–RF–CAS. The bulk $2LiBH_4$–MgH_2 was ground with $TiCl_3$–RF–CAS at a weight ratio of 1:2 in the mortar. Nanoconfinement was carried out by using a Sievert–type apparatus (a PCTPro–2000 from Hy–Energy LLC). The mixture of bulk $2LiBH_4$–MgH_2 and $TiCl_3$–RF–CAS was heated to 310 °C (5 °C/min) under a hydrogen pressure of 60 bar, kept

at 310 °C for 30 min, and cooled to room temperature. The sample was denoted as nanoconfined $2LiBH_4$–MgH_2–$TiCl_3$. For comparison, the nanoconfined $2LiBH_4$–MgH_2 without catalyst (1:2 weight ratio of bulk $2LiBH_4$–MgH_2: RF–CAS) was also prepared by the same procedures.

2.2. Characterizations

To characterize the texture parameters of the RF–CAS, $TiCl_3$–RF–CAS, and nanoconfined $2LiBH_4$–MgH_2–$TiCl_3$, N_2 adsorption–desorption measurements were carried out using a Nova 2000e surface area and pore size analyzer from Quantachrome. Prior to the measurements, a known amount of sample was degassed at 200 °C under vacuum for several hours. All samples were measured with a full adsorption and desorption isotherm in the pressure range of 0 to 1 p/p_0 at liquid nitrogen temperatures with nitrogen gas as an adsorbent. The measurement was programmed to continuously change the pressure ratio to 1 for adsorption, and to 0 for desorption. Data were analysed by the t–plot method [27–28], the Brunner Emmet Teller (BET) method [29], and the Barret Joyner Halenda (BJH) method, and the highest point of the isotherm measurement (where $p/p_0 \sim 1$) was used to calculate the total volume of the sample [30].

Scanning electron microscopy (SEM) and energy dispersive X–ray spectroscopy (EDS) were done by using an Auriga instrument from Zeiss, Germany and apparatus from EDAX Inc., USA, respectively. Smart SEM and EDS Genesis programs were used for morphological studies and elemental analysis, respectively. The powder samples were deposited onto the sample holder by using silver glue (in *n*–butylacetate) and continuously coated by palladium–gold sputtering with a current of 30 mA for 30 s under vacuum. An internal view of the nanoconfined $2LiBH_4$–MgH_2–$TiCl_3$ ($20 \times 20 \times 6$ μm^3) was produced by the focus ion beam (FIB) technique using a Canixon instrument from Orsay Physics, France. The specimen was irradiated by a gallium ion beam with an energy of 30 kV.

Coupled manometric–calorimetric measurements of nanoconfined $2LiBH_4$–MgH_2–$TiCl_3$ and $2LiBH_4$–$MgBu_2$ were carried out by connecting a high–pressure calorimeter (a Sensys DSC, Setaram) to a Sievert–type apparatus (a PCTPro–2000, Setaram & Hy–Energy). The high–pressure cell of the calorimeter, connected to the manometric instrument by a 1/8 in. stainless

steel tube, was loaded with ~ 13–25 mg of the powder samples in the glove box. Dehydrogenations were performed by heating the samples from room temperature up to 500°C with heating rates of 5 °C/min under 3 bar H_2 pressure. The calorimetric profiles were compiled by a Calisto software to obtain the peak temperatures.

The kinetic properties concerning dehydrogenation, rehydrogenation and cycling efficiency were studied by a carefully calibrated Sievert–type apparatus (a PCTPro–2000 from Hy–Energy LLC). The powder samples (~120 mg) were put into a high pressure–temperature vessel and transferred to the Sievert–type apparatus. Dehydrogenation of nanoconfined $2LiBH_4$–MgH_2–$TiCl_3$ was done at 425 °C (5 °C/min) under ~ 3.4 bar H_2. For rehydrogenation, the dehydrogenated powder was heated to 425 °C (5 °C/min) under hydrogen pressure in the range of 130–145bar and kept at 425 °C for 12 h. For comparison, nanoconfined $2LiBH_4$–MgH_2 without catalyst was also dehydrogenated and rehydrogenated by similar procedures.

In situ synchrotron radiation powder X–ray diffraction (SR–PXD) experiments were carried out at the MAX II Synchrotron, beamline I711 in the MAX–lab Research Laboratory, Lund, Sweden [31]. The powder diffraction patterns were recorded by a MAR165 CCD detector with a selected X–ray wavelength of 0.99917 Å. The sapphire capillaries were filled airtight with the powder samples under a purified argon atmosphere in the glovebox. After infiltration, dehydrogenation, and rehydrogenation, the powder samples of nanoconfined $2LiBH_4$–MgH_2–$TiCl_3$ were investigated by performing single scan X–ray diffraction. The infiltrated powder sample was dehydrogenated by heating to 435 °C (3°C/min) under 3.5 bar H_2, kept at 435 °C for 1 h, and cooled to room temperature. In the case of rehydrogenation, the dehydrogenated powder sample was heated to 435 °C (3 °C/min) under 100–120 bar H_2, kept at 435 °C for 1 h, and cooled to room temperature.

The powder samples of nanoconfined $2LiBH_4$–MgH_2–$TiCl_3$ (after rehydrogenation) and pristine $LiBH_4$ were identified by Fourier transform infrared (FTIR) spectroscopy using a Bruker Equinox 55. The mixture of sample powder and anhydrous KBr was ground in the mortar with a weight ratio of 10:1 (KBr: powder sample), and continuously pressed under a specific pressure to obtain a KBr pellet. The KBr pellet containing the sample was placed in the sample holder assembled in the direction of infrared radiation. The spectra were collected in the wavenumber range of 3000–450 cm^{-1} with 64 scans for both sample and background.

3. Results and discussion

3.1. Nanoconfinement of composite hydride $2LiBH_4$–MgH_2 and $TiCl_3$

To confirm the successful confinement of composite hydride $2LiBH_4$–MgH_2 and $TiCl_3$ in the nanoporous structure of RF–CAS, N_2 adsorption–desorption analysis was carried out. In this study, RF–CAS with a surface area, a pore diameter, and a total pore volume of 659 m^2/g, 26 nm, and 1.30 mL/g, respectively, was used (Table 1). After impregnation of $TiCl_3$, the surface area and microporous (pore size < 2 nm) volume of the RF–CAS decrease to 629.6m^2/g and 0.17 mL/g, respectively ($TiCl_3$–RF–CAS in Table 1). In contrast, the pore diameter and mesoporous (2 nm < pore size <50 nm) volume of $TiCl_3$–RF–CAS increase to 30.34 nm and 1.17 mL/g, respectively. This implies that $TiCl_3$ is successfully impregnated only in the microporous structure of RF–CAS. In the case of nanoconfined $2LiBH_4$–MgH_2–$TiCl_3$, significant decreases in the surface area and total pore volume to 43.5 m^2/g and 0.41 mL/g, respectively, with respect to $TiCl_3$–RF–CAS are achieved, confirming the nanoconfinement of $2LiBH_4$–MgH_2 in $TiCl_3$–RF–CAS (Table 1). Furthermore, the SEM–EDS experiments and FIB technique were also used to investigate the states of both $2LiBH_4$–MgH_2 and $TiCl_3$ in RF–CAS. Figure 1(A) reveals the surface morphology of nanoconfined $2LiBH_4$–MgH_2–$TiCl_3$, where the EDS results (Figure 1(B)) show that most of the components are carbon (C) and oxygen (O) from RF–CAS and oxidation in air, respectively. Moreover, small amounts of magnesium (Mg) and gold (Au) representing MgH_2 and palladium–gold spattering, respectively, are detected. To confirm the nanoconfinement of both $2LiBH_4$–MgH_2 and $TiCl_3$ in RF–CAS, a specimen of nanoconfined sample was irradiated by a gallium ion beam using the FIB technique to explore the internal areas of the RF–CAS matrices (Figure 1(C)). From the EDS results of the area in the red frame (Figure 1(C)), C and O are still the main elements as found on the surface, together with Mg and gallium (Ga) from MgH_2 and Ga–ion (FIB technique), respectively (Figure 1(D)). However, it should be noted that the exposure of chlorine (Cl) and Ti signals (Figure 1(D)) verifies that $TiCl_3$ is successfully impregnated in the porous structure of RF–CAS. Figures 1(B) and (D) assure the presence of MgH_2 both on the surface and in the pores of RF–CAS. Due to the limitation of the EDS experiment, which is not sensitive to light elements, the existences of lithium (Li) and boron (B) from $LiBH_4$ cannot be detected. Nevertheless, the nanoconfinement of $LiBH_4$ in RF–CAS is confirmed afterward by the SR–PXD results (Figure 5).

The amount of each component in nanoconfined samples with and without $TiCl_3$ was also calculated by the weight difference before and after confinement. Table 2 shows that nanoconfined $2LiBH_4$–MgH_2 contains 66.5, 20.7, and 12.8 wt. % of RF–CAS, $LiBH_4$, and MgH_2, respectively, while nanoconfined $2LiBH_4$–MgH_2–$TiCl_3$ has 65.1, 21.0, 12.3, and 1.6 wt. % of RF–CAS, $LiBH_4$, MgH_2, and $TiCl_3$, respectively. The mole ratios of $LiBH_4$:MgH_2 of both the nanoconfined samples are approximately 2:1. Regarding the dehydrogenation mechanism of $2LiBH_4$–MgH_2 (reaction (1)), 11.43 wt. % H_2 is reversible. Therefore, theoretical hydrogen storage capacities of 3.83 and 3.80 wt. % H_2 are calculated for nanoconfined $2LiBH_4$–MgH_2 and $2LiBH_4$–MgH_2–$TiCl_3$, respectively (Table 2).

$$2LiBH_{4(l)} + MgH_{2(s)} \longleftrightarrow 2LiH_{(s)} + MgB_{2(s)} + 4H_{2(g)} \quad (1)$$

3.2. Dehydrogenation profiles

The dehydrogenation behaviours of nanoconfined samples both with and without $TiCl_3$ were studied by coupled manometric–calorimetric measurements. Figures 2(A) and (B) show the polymeric phase transformations of the nanoconfined samples at 105 °C. For melting of $LiBH_4$, nanoconfined $2LiBH_4$–MgH_2 reveals an endothermic peak at 270 °C. In the case of nanoconfined $2LiBH_4$–MgH_2–$TiCl_3$, the onset temperature at ~ 250 °C belongs not only to $LiBH_4$ melting, but also to partial dehydrogenation, as indicated by the reduction of the manometric response. By heating the samples, nanoconfined $2LiBH_4$–MgH_2 releases hydrogen in the temperature range of 275–383°C (Figure 2(A)), while that of the nanoconfined $2LiBH_4$–MgH_2–$TiCl_3$ begins at 250 °C, together with $LiBH_4$ melting as mentioned above, and completes at 396°C (Figure 2(B)). The manometric results of both nanoconfined samples present single–step dehydrogenation (Figures 2 (A) and (B)), corresponding to the previous studies of nanoconfined $2LiBH_4$–MgH_2 in RF–CAS with 31 nm pore size [4]. Compared with ball–milled $2LiBH_4$–MgH_2–1 mol % $TiCl_3$ sample, showing an onset temperature of 300 °C for dehydrogenation [12], it can be remarked that the dehydrogenation temperature decreases by 50 ° C after nanoconfinement (nanoconfined $2LiBH_4$–MgH_2–$TiCl_3$ starts desorption at 250 °C). The amount of hydrogen released from the nanoconfined samples of $2LiBH_4$–MgH_2 and $2LiBH_4$–MgH_2–$TiCl_3$ are 3.35 and 3.58 wt. % H_2, respectively, approaching the theoretical hydrogen storage capacities (Table 2). Although the hydrogen desorption of nanoconfined $2LiBH_4$–

MgH_2–$TiCl_3$ completes at a higher temperature (396°C) than that of nanoconfined $2LiBH_4$–MgH_2 (383°C), it starts to desorb hydrogen at a lower temperature (250 °C). Furthermore, it should be noted that in the same desorption temperature range (room temperature to ~500 °C), nanoconfined $2LiBH_4$–MgH_2–$TiCl_3$ releases 94.2 % of the theoretical H_2 storage capacity (3.58 wt. % H_2), while that of nanoconfined $2LiBH_4$–MgH_2 gives only 87.5 % (3.35 wt. % H_2). This faster dehydrogenation rate in the same temperature range suggests kinetic improvement after $TiCl_3$ impregnation.

3.3. Kinetic properties and hydrogen storage capacity

The kinetics, reversibility, and hydrogen reproducibility were evaluated using a Sievert–type apparatus. Four hydrogen release (T = 425 °C, $p(H_2)$ = 3.4 bar) and uptake (T = 425 °C, $p(H_2)$ = 130–145 bar) cycles were carried out on both nanoconfined $2LiBH_4$–MgH_2 and $2LiBH_4$–MgH_2–$TiCl_3$. The hydrogen back pressure (3.4 bar) used during dehydrogenation was to avoid the formation of an intermediate $Li_2B_{12}H_{12}$ phase and to encourage MgB_2 formation, considered to be crucial for the reversibility of a $2LiBH_4$–MgH_2 based system (reaction (1)) [32]. Moreover, at least 3 bar H_2 is required to suppress the individual decomposition of $LiBH_4$ before the occurrence of reaction (1) to produce LiH and MgB_2. However, the higher the hydrogen back pressure, the lower the dehydrogenation rate. Therefore, a hydrogen back pressure between 3–4 bar was used. Figure 3 shows that both nanoconfined samples have comparable H_2 storage capacities of ~ 3.6 wt. % H_2 (10.8 wt. % H_2 with respect to the hydride content) during the 1st dehydrogenation. The amount of hydrogen desorbed from both nanoconfined samples during the 1st cycle approaches the theoretical values (Table 2) and those from manometric–calorimetric results (Figure 2). Moreover, it should be noted that desirable kinetics is obtained from nanoconfined $2LiBH_4$–MgH_2–$TiCl_3$, where the total hydrogen content is released approximately twice as fast as the sample without a catalyst. Afterward, the dehydrogenated samples from the 1st cycle was rehydrogenated at 425 °C under 130 bar H_2. For the 2nd cycles, the superior kinetics and greater amount of hydrogen reproduced are obviously achieved from nanoconfined $2LiBH_4$–MgH_2–$TiCl_3$. For instance, after 8 h nanoconfined $2LiBH_4$–MgH_2–$TiCl_3$ releases 3.25 wt. % H_2, while that of nanoconfined $2LiBH_4$–MgH_2 is less than 3 wt. % H_2 (Figure 3). Due to the inferior amount of hydrogen released in the 2nd cycle as compared with the 1st cycle, the hydrogen pressure during the 2nd rehydrogenation was increased to 145 bar (425 °C). In the 3rd

and 4th cycles, nanoconfined $2LiBH_4–MgH_2–TiCl_3$ reveals comparable kinetics and H_2 storage capacity of ~ 3.6–3.75 wt. % H_2 after 15 h. With regard to nanoconfined $2LiBH_4–MgH_2$, a similar dehydrogenation phenomenon is also achieved during the 3rd and 4th cycles, where comparable kinetics is obtained. Interestingly, the superior kinetics and H_2 storage capacity are still accomplished during the 3rd and 4th cycles of nanoconfined $2LiBH_4–MgH_2–TiCl_3$, that is, after 14 h, nanoconfined $2LiBH_4–MgH_2–TiCl_3$ releases ~ 3.75 wt. % H_2, while that of nanoconfined $2LiBH_4–MgH_2$ is ~ 3.4 wt. % H_2 (the 4th cycle in Figure 3). Thus, it can be concluded from the titration results that the kinetics of nanoconfined $2LiBH_4–MgH_2$ is improved after $TiCl_3$ impregnation in accordance with the coupled manometric–calorimetric results. In this regard, the small amount of $TiCl_3$ (1.6 wt. % with respect to RF–CAS) not only improves significantly the kinetics of the system, but also reproduces the highest H_2 storage capacity after four cycles of 3.6–3.75 wt. % (95–98.6 % of theoretical H_2 storage capacity), which is greater than that of the nanoconfined sample without catalyst (~3.5 wt. % H_2, i.e., 91.4 % of theoretical H_2 storage capacity).

To clearly show the influence of $TiCl_3$ on the kinetics of nanoconfined $2LiBH_4–MgH_2$, the normalized hydrogen desorption profiles are considered. From Figure 4, nanoconfined $2LiBH_4–MgH_2–TiCl_3$ produces the greatest dehydrogenation rate at all cycles over nanoconfined and bulk $2LiBH_4–MgH_2$ samples. It is found that during the 1st and 2nd cycles, nanoconfined $2LiBH_4–MgH_2–TiCl_3$ requires ~ 2 and 4.5 h, respectively, to release 95 % of the total hydrogen content, while the times for nanoconfined $2LiBH_4–MgH_2$ (~ 1 and 7 h, respectively) and bulk material (~ 23 and 22 h, respectively) are considerably longer. Concerning the ball–milled $2LiBH_4–MgH_2–1$ mol% $TiCl_3$ sample reported elsewhere [12], ~5 h (at 450 °C) was required to complete 95 % of the two–step dehydrogenation. Therefore, nanoconfined $2LiBH_4–MgH_2–TiCl_3$ provides a considerable kinetic improvement at a lower temperature (425 °C) based on the single–step reaction and a five times faster dehydrogenation rate. During the 3rd and 4th cycles, the complete dehydrogenations of nanoconfined $2LiBH_4–MgH_2–TiCl_3$ are accomplished after 17.5 h, while nanoconfined $2LiBH_4–MgH_2$ needs up to 22.5 h (3rd cycle) (Figure 4). Interestingly, the kinetics of nanoconfined $2LiBH_4–MgH_2–TiCl_3$ seems to be stable after the 3rd cycle, as shown by the overlapped kinetic plots of the 3rd and 4th cycles.

3.4. Reaction mechanisms and reversibility

Reaction mechanisms during each process of nanoconfined $2LiBH_4–MgH_2–TiCl_3$ were investigated by *in situ* synchrotron radiation powder X–ray diffraction (SR–PXD) and Fourier transform infrared spectroscopy (FTIR). A single scan X–ray diffraction pattern was obtained after each state of melt infiltration, dehydrogenation and rehydrogenation. From Figure 5(a), the broad region in agreement with a graphite–like structure of RF–CAS is observed in the 2θ range of 10–15° [4, 33]. Furthermore, the Bragg diffraction peaks of α–$LiBH_4$, MgH_2, TiB_2, and LiCl, with no presence of $TiCl_3$, are observed. This implies that during melt infiltration $LiBH_4$ partially reacts with all the $TiCl_3$ to produce TiB_2 and LiCl, while MgH_2 does not undergo any reaction. With respect to the SEM–EDS results of nanoconfined $2LiBH_4–MgH_2–TiCl_3$, $TiCl_3$ is completely impregnated in the RF–CAS matrices after melt infiltration, as indicated by significant appearances of Ti and Cl signals (Figures 1(C) and (D)). Therefore, the reaction between $LiBH_4$ and $TiCl_3$ (in RF–CAS) confirms the nanoconfinement of $LiBH_4$ in RF–CAS. On the basis of the clear diffraction peaks of $LiBH_4$ and the reaction between $LiBH_4$ and $TiCl_3$, it can be hypothesized that $LiBH_4$ is both on the surface and in the nanopores of RF–CAS after infiltration as in the case of MgH_2. Afterward, the dehydrogenated sample, obtained from heating the infiltrated sample to 435 °C under 3.5 bar H_2 and keeping it at isothermal and isobaric conditions for 1 h, exhibits the diffraction peaks of Mg and MgO as well as broad region corresponding to the graphite–like structure of RF–CAS (Figure 5(b)). This suggests the successful dehydrogenation of MgH_2 to Mg. For MgO, it could be due to the oxidation of Mg from a small amount of oxygen in the sapphire capillary. In the case of $LiBH_4$, dehydrogenation is also accomplished, as confirmed by the disappearance of its diffraction peaks as well as the hydrogen content released from titration results (3.6 wt. % H_2). However, the diffraction peaks of the dehydrogenation products (e.g., LiH and MgB_2) cannot be determined due to their complete nanoconfinement in RF–CAS [18]. For rehydrogenation, the dehydrogenated sample was heated to 435 °C (3 °C/min) under 100–120 bar H_2, kept at this temperature for 1 h, and cooled to room temperature. In Figure 5 (c), the diffraction peaks of MgH_2 are presented, together with those of MgO gained during dehydrogenation. In order to conclude that the system is reversible, not only the formation of MgH_2 after rehydrogenation needs to be confirmed, but also the formation of $LiBH_4$ must be established. However, due to the fact that nanoconfined $LiBH_4$ is inactive for X–ray diffraction, no traces of $LiBH_4$ were detected in the diffraction pattern after rehydrogenation.

Therefore, an alternative investigation by FTIR was performed. Figure 6(a) shows the characteristic peaks of commercial $LiBH_4$ infrared absorption at 2390, 2302, 2222, and 1127 cm^{-1}[34–35]. From Figure 6(b), the rehydrogenated sample of nanoconfined $2LiBH_4$–MgH_2–$TiCl_3$ shows all the characteristic peaks corresponding to pristine $LiBH_4$, as revealed in Figure 6(a). Thus, the formations of MgH_2 and $LiBH_4$ after rehydrogenation prove the reversibility of nanoconfined $2LiBH_4$–MgH_2–$TiCl_3$ as a hydrogen storage material.

4. Conclusion

A hydrogen storage material of nanoconfined $2LiBH_4$–MgH_2–$TiCl_3$ was prepared by $TiCl_3$ solution impregnation and $2LiBH_4$–MgH_2 melt infiltration. Nanoconfinement of both $TiCl_3$ and bulk $2LiBH_4$–MgH_2 was confirmed by N_2 adsorption–desorption and SEM–EDS measurements. The reaction mechanisms, revealed by SR–PXD and FTIR experiments, assured the reversibility of this hydrogen storage material. The kinetics improved significantly by adding only 1.6 wt. % $TiCl_3$ (with respect to RF–CAS content) in the nanoconfined $2LiBH_4$–MgH_2. For example, nanoconfined $2LiBH_4$–MgH_2–$TiCl_3$ released total hydrogen within 2 h during the 1st cycle, while nanoconfined and bulk $2LiBH_4$–MgH_2 required 4 and more than 25 h, respectively. Moreover, the hydrogen reproducibility of nanoconfined $2LiBH_4$–MgH_2–$TiCl_3$ after four release and uptake cycles was maintained at 3.6–3.75 wt. % (95–98.6 % of theoretical hydrogen storage capacity), which was higher than that of nanoconfined $2LiBH_4$–MgH_2 in the same temperature and time ranges. These results confirmed that the small amount of $TiCl_3$ present in the nanoconfined sample not only improved the kinetics of the system, but it also promoted hydrogen reproducibility after several cycles.

5. Acknowledgements

The authors would like to acknowledge Suranaree University of Technology, Thailand (under the project title of “Development of materials for sustainable environment and energy”, SUT1–102–54–12–20) as well as the project “Development, Upscaling and Testing of Nanocomposite Materials for Hydrogen Storage” in the frame of the German National Innovation Program on Hydrogen and Fuel Cell technology for financial support. We acknowledge Dr. Yngve Cerenius for his kind help and for providing beam time at the I711 beamline (Max–lab, Lund, Sweden). Also, we would like to thank Mr. Silvio Neumann

(Institute of Polymer Research, Helmholtz–Zentrum Geesthacht) for assistance doing the FTIR experiments.

Table and Figures captions

Table 1 Texture parameters of RF–CAS, $TiCl_3$–RF–CAS, and nanoconfined $2LiBH_4$–MgH_2–$TiCl_3$.

Table 2 Calculated amounts of all components, $LiBH_4$:MgH_2 mole ratio, and theoretical hydrogen storage capacities of the nanoconfined samples.

Figure 1. SEM micrographs and elemental analysis (EDS results) of the nanoconfined $2LiBH_4$–MgH_2–$TiCl_3$ on the surface areas (A) and (B), respectively, and in the internal areas (in the red frame) (C) and (D), respectively.

Figure 2.Coupled manometric–calorimetric analysis of nanoconfined samples of $2LiBH_4$–MgH_2 (A) and $2LiBH_4$–MgH_2–$TiCl_3$ (B).

Figure 3. Dehydrogenation profiles and cycling efficiency of nanoconfined samples of $2LiBH_4$–MgH_2 and $2LiBH_4$–MgH_2–$TiCl_3$.

Figure 4. Normalized hydrogen desorption profiles of bulk $2LiBH_4$–MgH_2 and nanoconfined samples of $2LiBH_4$–MgH_2 and $2LiBH_4$–MgH_2–$TiCl_3$.

Figure 5. SR–PXD single scans of the nanoconfined $2LiBH_4$–MgH_2–$TiCl_3$ after melt infiltration (a), after dehydrogenation (b), and after rehydrogenation (c).

Figure 6. FTIR spectra of pristine $LiBH_4$ (a) and nanoconfined $2LiBH_4$–MgH_2–$TiCl_3$ after rehydrogenation (b).

References

[1] Fang ZZ, Kang XD, Wang P. Improved hydrogen storage properties of $LiBH_4$ by mechanical milling with various carbon additives. Int J Hydrogen Energ 2010; 35: 8247–8252.

[2] Xu J, Cao J, Yu X, Zou Z, Akins DL, Yang H. Enhanced catalytic hydrogen release of $LiBH_4$ by carbon–supported Pt nanoparticle. J Alloys Compd 2010; 490: 88–92.

[3] Bösenberg U, Doppiu S, Mosegaard L, Berkhordarian G, Eigen N, Borgschulte A, et al. Hydrogen sorption properties of MgH_2–$LiBH_4$ composites. Acta Materialia 2007; 55: 3951–3958.

[4] Gosalawit–Utke R, Nielsen TK, Saldan I, Laipple D, Cerenius Y, Jensen TR, et al. Nanoconfined $2LiBH_4$–MgH_2 Prepared by Direct Melt Infiltration into Nanoporous Materials. J Phys Chem C 2011; 115: 10903–10910.

[5] Gross AF, Vajo JJ, Van Atta SL, Olson GL. Enhanced Hydrogen Storage Kinetics of $LiBH_4$ in Nanoporous Scaffold. J Phys Chem C 2008; 112: 5651–5657.

[6] Zaluska A, Zaluski L, Ström–Olsen JO. Nanocrystalline magnesium for hydrogen storage.J Alloys Compd 1999; 288: 217–225.

[7] Lu J, Choi YJ, Fang ZZ, Sohn HY, Rönnebro E. Hydrogen Storage Properties of Nanosized MgH_2–$0.1TiH_2$ Prepared by Ultrahigh–Energy–High–Pressure Milling. J Am Chem Soc 2009; 131: 15843–15852.

[8] Hao S, Sholl DS. Effect of TiH_2–induced Strain on Thermodynamics of Hydrogen Release from MgH_2. J Phys Chem C 2012; 116: 2045–2050.

[9] Yu XB, Grant DM, Walker GS. Dehydrogenation of $LiBH_4$ Destabilized with Various Oxides. J Phys Chem C 2009; 113: 17945–17949.

[10] Mao JF, Wu Z, Chen TJ, Weng BC, Xu NX, Huang TS, et al. Improved Hydrogen Storage of $LiBH_4$ Catalyzed Magnesium. J Phys Chem C 2007; 111: 12495–12498.

[11] Yu XB, Grant DM, Walker GS. A new dehydrogenation mechanism for reversible multicomponent borohydride systems – The roll of Li–Mg alloys. Chem. Commun 2006; 37: 3906–3908.

[12] Sridechprasat P, Suttisawat Y, Rangsunvigit P, Kitiyana B, Kulprathipanja S. Catalyzed $LiBH_4$ and MgH_2 mixture for hydrogen storage. Int J Hydrogen Energ 2011; 36; 1200–1205.

[13] Liu BH, Zhang BJ, Jiang Y. Hydrogen storage performance of $LiBH_4$+1/2MgH_2composites improved by Ce–based additive. Int J Hydrogen Energ 2011; 36: 5418–5424.

[14] Gross AF, Ahn CC, Van Atta SL, Liu P, Vajo JJ. Fabrication and hydrogen sorption behavior of nanoparticulate MgH_2 incorporated in a porous carbon host. Nanotechnology 2009; 20: 204005.

[15] Paskevicius M, Tian HY, Sheppard DA, Webb CJ, Pitt MP, Gray EM, et al. Magnesium Hydride Formation within Carbon Aerogel. J Phys Chem C 2011; 115: 1757–1766.

[16] Nielsen TK, Manickam K, Hirscher M, Besenbacher F, Jensen TR. Confinement of MgH_2Nanocluster within Nanoporous Aerogel Scaffold Materials. ACS Nano 2009; 3: 3521–3528.

[17] Gao J, Adelhelm P, Verkuijlen MHW, Rongeat C, Herrich M, van Bentum PJM, et al. Confinement of $NaAlH_4$ in Nanoporous Carbon: Impact on H_2 Release, Reversibility, and Thermodynamics. J Phys Chem C 2010; 114: 4675–4682.

[18] Gosalawit–Utke R, Nielsen TK, Pranzas K, Saldan I, Pistidda C, Karimi F, et al. 2$LiBH_4$–MgH_2 in a Resorcinol–Furfural Carbon Aerogel Scaffold for Reversible Hydrogen Storage. J Phys Chem C 2011; 116: 1526–1534.

[19] Nielsen TK, Bösenberg U, Gosalawit R, Dornheim M, Cerenius Y, Besenbacher F, et al. Reversible Nanoconfined Chemical Reaction. ACS Nano 2010; 4: 3903–3908.

[20] Mulas G, Campesi R, Garroni S, Napolitano E, Milanese C, Dolci F, et al. Hydrogen storage in 2$NaBH_4$–MgH_2 mixtures: Destabilization by additives and nanoconfinement. J Alloys Compd 2012; 536: S236–S240.

[21] Lee HS, Lee YS, Suh JY, Kim M, Yu JS, Cho YW. Enhanced Desorption and Absorption Properties of Eutectic $LiBH_4$–$Ca(BH_4)_2$ Infiltrated into Mesoporous Carbon. J Phys Chem C 2011; 115: 20027–20035.

[22] Nielsen TK, Polanski M, Zasada D, Javadian P, Besenbacher F, Bystrzycki J, et al. Improved Hydrogen Storage Kinetics of Nanoconfined $NaAlH_4$ Catalyzed with $TiCl_3$ Nanoparticles. ACS Nano 2011; 5: 4056–4064.

[23] Bösenberg U, Vainio U, Pranzas PK, von Colbe JMB, Goerigk G, Weiter E, et al. On the chemical state and distribution of Zr– and V–based additives in reactive hydride composites. Nanotechnology 2009; 20: 204003.

[24] Deprez E, Munoz–Marquez MA, Roldan MA, Prestipino C, Palomares FJ, Minella CB, et al. Oxidation State and Local Structure of Ti–Based Additives in the Reactive Hydride Composite $2LiBH_4$–MgH_2. J Phys Chem C 2010; 114: 3309–3317.

[25] Fan MQ, Sun LX, Zhang Y, Xu F, Zhang J, Chu HL. The catalytic effect of additive Nb_2O_5 on the reversible hydrogen storage performance of $LiBH_4$–MgH_2 composite. Int J Hydrogen Energ 2008; 33:74–80.

[26] Li WC, Lu AH, Weidenthaler C, Schüth F. Hard–Templating Pathway To Create Mesoporous Magnesium Oxide. Chem Mater 2004; 16: 5676–5681.

[27] Halsey G. Physical Adsorption on Non–Uniform Surfaces. J Chem Phys 1948; 16: 931–938.

[28] de Boer JH, Linsen BG, PlasTh, Zondervan GJ. Studies on pore systems in catalysts: VII. Description of the pore dimension of carbon blacks by the *t* method. J Catal 1969; 4: 649–653.

[29] Brunauer S, Emmet P, Teller E. Adsorption of Gases in Multimolecular Layers. J Am Chem Soc 1939; 60: 309–319.

[30] Barrett EP, Joyner LG, Halenda PP. The Determination of Pore Volume and Area Distributions in Porous Substances. I. Computations from Nitrogen Isotherms. J Am Chem Soc 1951; 73: 373–380.

[31] Cerenius Y, Ståhl K, Svesson LA, Ursby T, Oskarsson Å, Albertsson J, et al. The crystallography beamline I711 at MAX II. J Synchrotron Rad 2000; 7: 203–208.

[32] Yan Y, Li HW, Maekawa H, Miwa K, Towata S, Orimo S. Formation of Intermediate Compound $Li_2B_{12}H_{12}$ during the Dehydrogenation Process of the $LiBH_4$–MgH_2 System. J Phys Chem C 2011; 115: 19419–19423.

[33] Li J, Wang X, Huang Q, Gamboa S, Sebastian PJ. Studies on preparation and performances of carbon aerogel electrodes for the application of supercapacitor. J Power Sources 2006; 158: 784–788.

[34] Wan X, Shaw LL. Novel dehydrogenation properties derived from nanoscale $LiBH_4$. Acta Materialia 2011; 59: 4606–4615.

[35] Wu X, Wang X, Cao G, Li S, Ge H, Chen L, et al. Hydrogen storage properties of $LiBH_4$–Li_3AlH_6 composites. J Alloys Compd 2012; 517: 127–131.

Highlights

- $TiCl_3$ doped in nanoconfined $2LiBH_4$-MgH_2 via simple solution impregnation technique
- At least twice faster desorption kinetics obtained from only 1.6 wt. % $TiCl_3$ doping
- Up to 98.6 % H_2 content reproduced after four H_2 release and uptake cycles

Table 1

Samples	S_{BET} **(m^2/g)**	D_{max} **(nm)**	V_{micro} **(mL/g)**	V_{meso} **(mL/g)**	V_{total} **(mL/g)**
RF–CAS	659.0	26.0	0.19	1.10	1.30
$TiCl_3$–RF–CAS	629.6	30.3	0.17	1.17	1.35
Nanoconfined $2LiBH_4$–MgH_2–$TiCl_3$	43.5	30.1	0	0.45	0.41

Table 2

Nanoconfined samples	**Amount of components (wt. %)**				**Molar ratio of $LiBH_4$:MgH_2**	**Theoretical H_2 storage capacities (wt. % H_2)**
	RF–CAS	**$LiBH_4$**	**MgH_2**	**$TiCl_3$**		
$2LiBH_4$–MgH_2–RF	66.5	20.7	12.8	-	2:1	3.83
$2LiBH_4$–MgH_2–$TiCl_3$	65.1	21.0	12.3	1.6	2:1	3.80

(A)

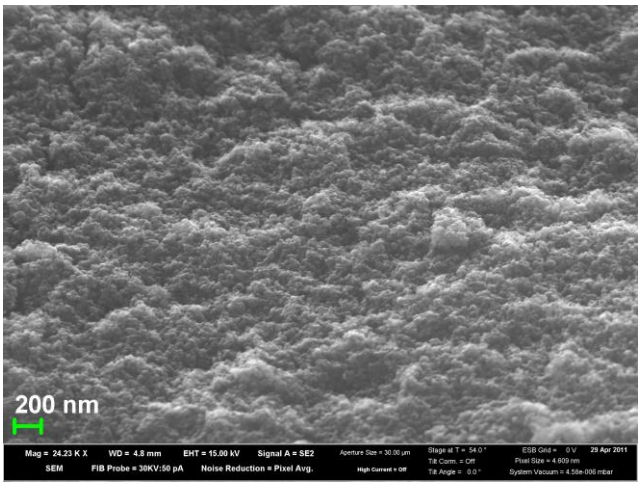

(B)

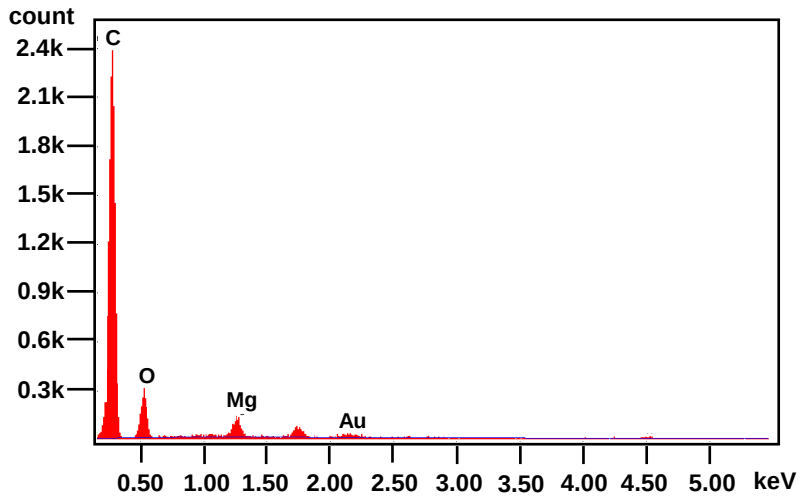

(C)

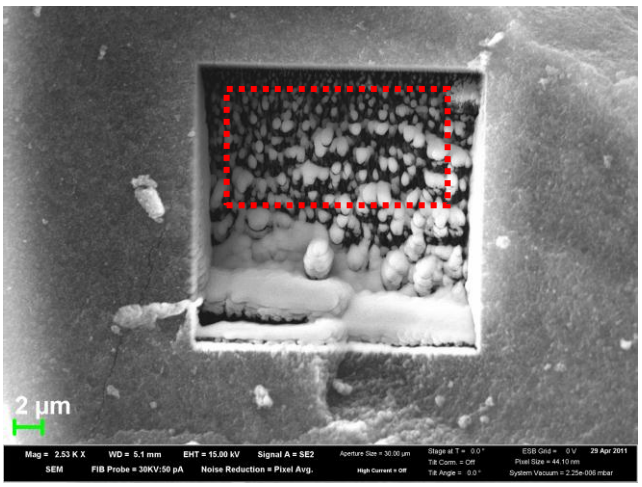

(D)

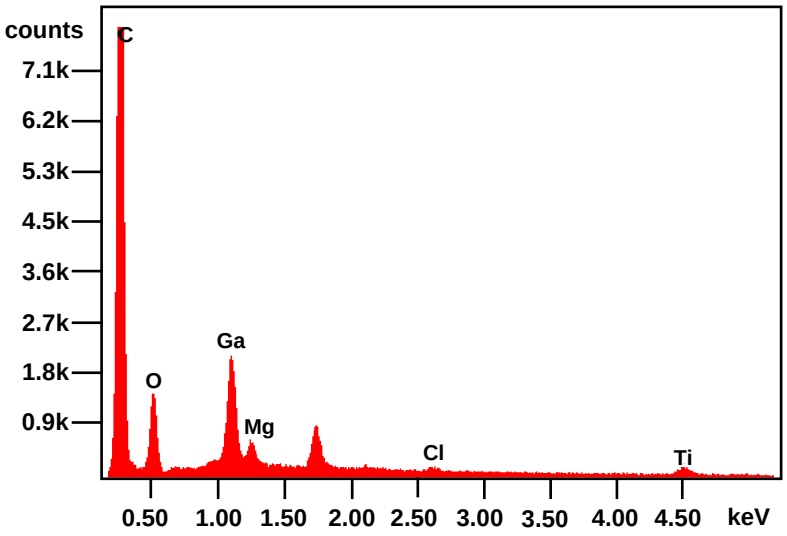

Figure 1

(A)

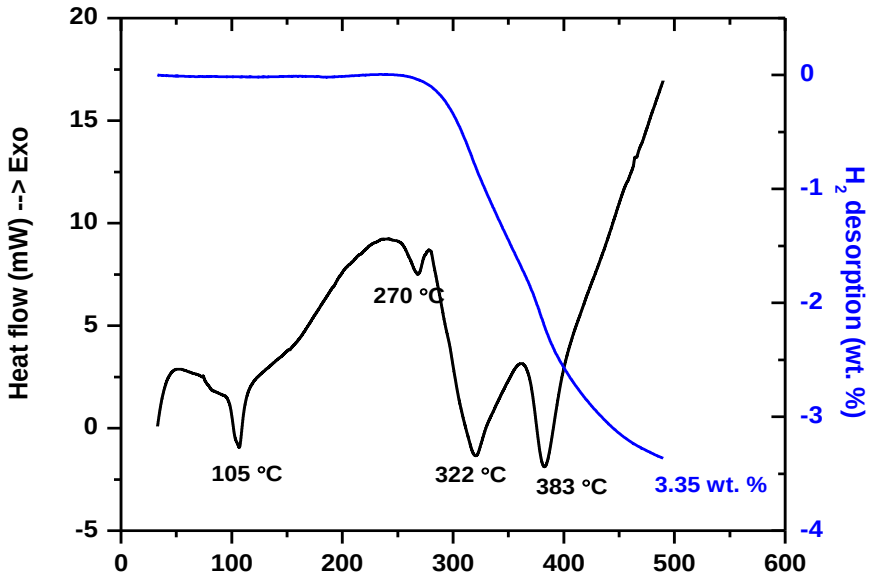
Heat flow (mW) --> Exo
H2 desorption (wt. %)
105 °C
270 °C
322 °C
383 °C
3.35 wt. %
Temperature (°C)

(B)

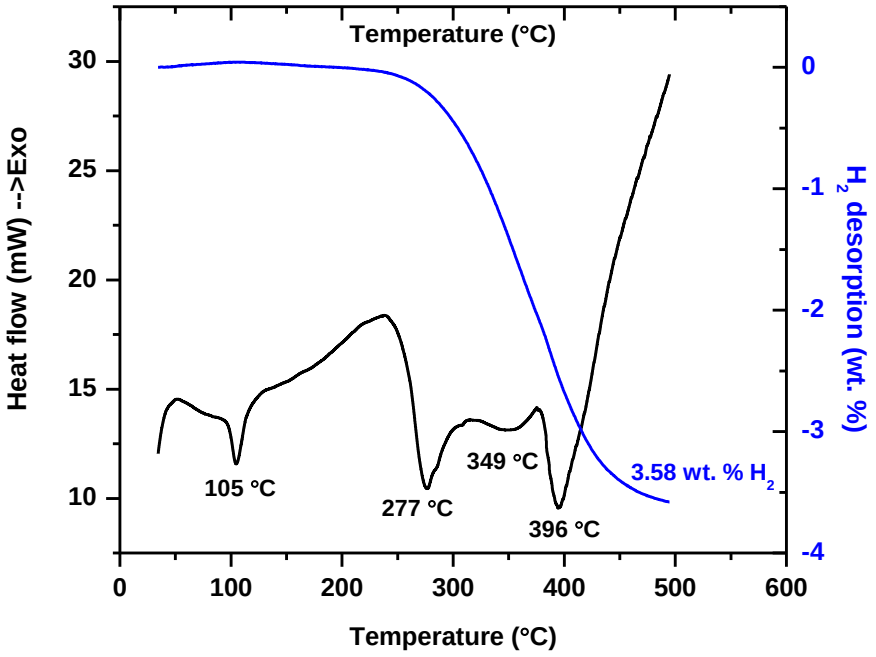
Heat flow (mW) -->Exo
H2 desorption (wt. %)
105 °C
277 °C
349 °C
396 °C
3.58 wt. % H2
Temperature (°C)

Figure 2

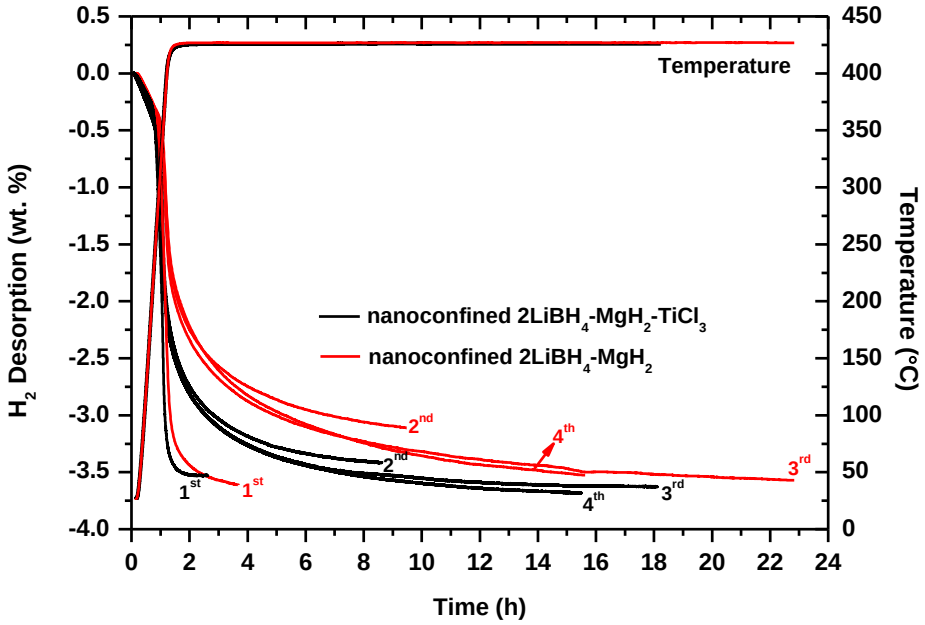
H2 Desorption (wt. %)
Temperature (°C)
Time (h)
Temperature
nanoconfined 2LiBH4-MgH2-TiCl3
nanoconfined 2LiBH4-MgH2
1st
2nd
3rd
4th
1st
2nd
3rd
4th

Figure 3

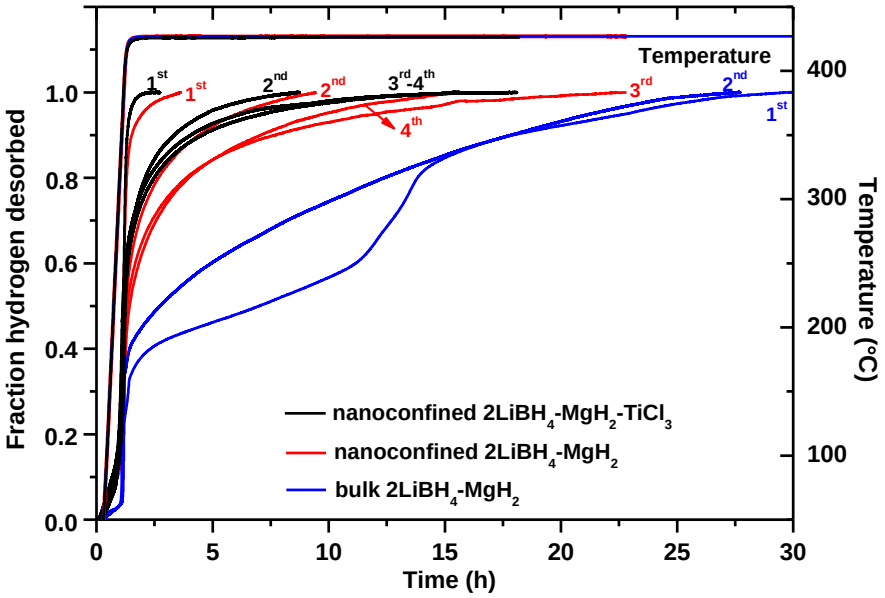
Fraction hydrogen desorbed
Temperature (°C)
Time (h)
Temperature
1st
1st
2nd
2nd
3rd-4th
4th
3rd
2nd
1st
nanoconfined 2LiBH4-MgH2-TiCl3
nanoconfined 2LiBH4-MgH2
bulk 2LiBH4-MgH2
0.0
0.2
0.4
0.6
0.8
1.0
0
5
10
15
20
25
30
100
200
300
400

Figure 4

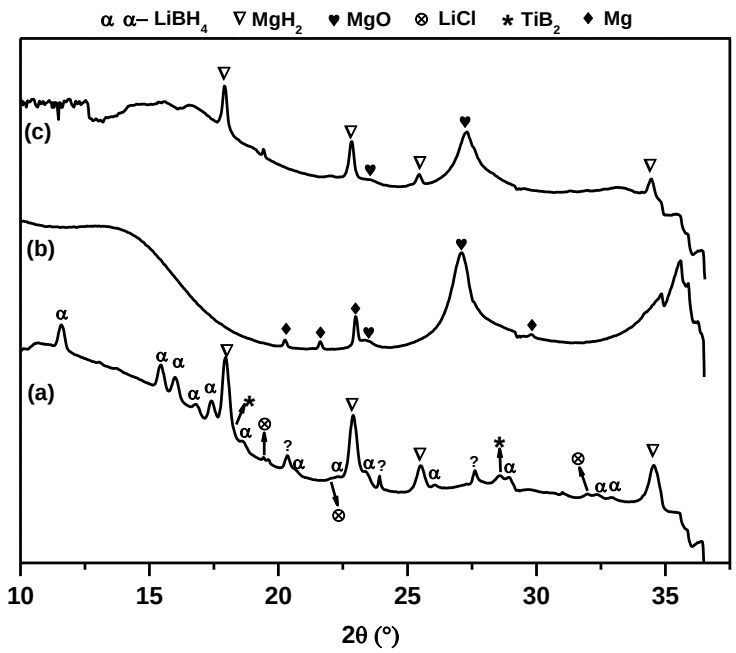

Figure 5

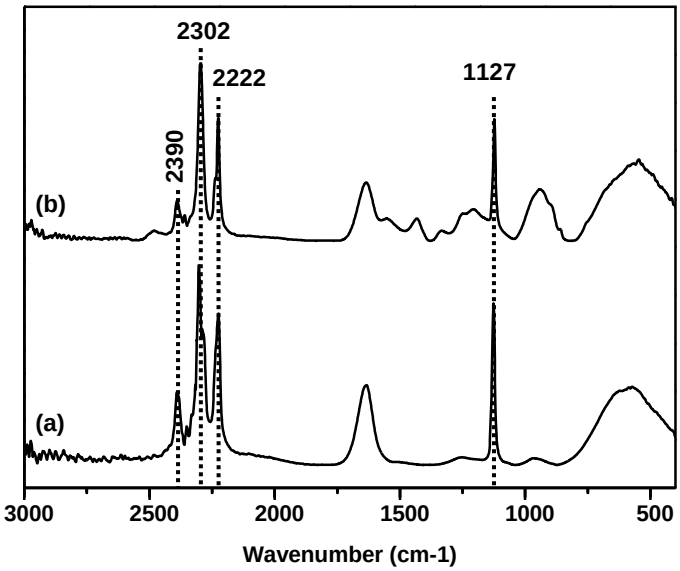
2302
2222
1127
2390
(b)
(a)
3000
2500
2000
1500
1000
500
Wavenumber (cm-1)

Figure 6